

## Article

# Highly Efficient CO<sub>2</sub> Capture and Utilization of Coal and Coke-Oven Gas Coupling for Urea Synthesis Process Integrated with Chemical Looping Technology: Modeling, Parameter Optimization, and Performance Analysis

Qiang Wang <sup>1</sup>, Yong Yang <sup>2</sup>  and Huairong Zhou <sup>2,\*</sup><sup>1</sup> The 404 Company Limited, China National Nuclear Corporation, Jiayuguan 735100, China<sup>2</sup> College of Petrochemical Technology, Lanzhou University of Technology, Lanzhou 730050, China

\* Correspondence: zhouhr@lut.edu.cn

**Abstract:** The resource endowment structure of being coal-rich and oil-poor makes China's production of coal-based ammonia and urea, with a low production cost and a good market, a competitive advantage. However, the process suffers from high CO<sub>2</sub> emissions and low energy efficiency and carbon utilization efficiency due to the mismatch of hydrogen-to-carbon ratio between raw coal and chemicals. Based on the coal-to-urea (CTU) process and coal-based chemical looping technology for urea production processes (CTU<sub>CLAS&H</sub>), a novel urea synthesis process from a coal and coke-oven gas-based co-feed chemical looping system (COG-CTU<sub>CLAS&H</sub>) is proposed in this paper. By integrating chemical looping air separation and chemical looping hydrogen production technologies and the synergies between coal gasification, low-energy consumption CO<sub>2</sub> capture and CO<sub>2</sub> utilization are realized; the excess carbon emissions of the CTU process are avoided through coupling the pressure swing adsorption of COG, and the low carbon emissions of the proposed system are obtained. In this work, the novel process is studied from three aspects: key unit modeling, parameter optimization, and technical-economic evaluation. The results show that COG-CTU<sub>CLAS&H</sub> achieves the highest system energy efficiency (77.10%), which is much higher than that of the CTU and CTU<sub>CLAS&H</sub> processes by 40.03% and 32.80%, respectively, when the optimized ratio of COG to coal gasified gas is 1.2. The carbon utilization efficiency increases from 35.67% to 78.94%. The product cost of COG-CTU<sub>CLAS&H</sub> is increased compared to CTU and CTU<sub>CLAS&H</sub>, mainly because of the introduction of COG, but the technical performance advantages of COG-CTU<sub>CLAS&H</sub> make its economic benefits obvious, and the internal rate of return of COG-CTU<sub>CLAS&H</sub> is 26%, which is larger than the 14% and 16% of CTU and CTU<sub>CLAS&H</sub>, respectively. This analysis will enable a newly promising direction of coal and COG-based co-feed integrated chemical looping technology for urea production.

**Keywords:** highly efficient CO<sub>2</sub> capture and utilization; chemical looping technology; pressure swing adsorption; conceptual design; technoeconomic analysis



**Citation:** Wang, Q.; Yang, Y.; Zhou, H. Highly Efficient CO<sub>2</sub> Capture and Utilization of Coal and Coke-Oven Gas Coupling for Urea Synthesis Process Integrated with Chemical Looping Technology: Modeling, Parameter Optimization, and Performance Analysis. *Processes* **2023**, *11*, 960. <https://doi.org/10.3390/pr11030960>

Academic Editor: Jean-Pierre Corriou

Received: 23 February 2023

Revised: 16 March 2023

Accepted: 18 March 2023

Published: 21 March 2023



**Copyright:** © 2023 by the authors. Licensee MDPI, Basel, Switzerland. This article is an open access article distributed under the terms and conditions of the Creative Commons Attribution (CC BY) license (<https://creativecommons.org/licenses/by/4.0/>).

## 1. Introduction

As the most widely used nitrogen fertilizer, urea plays a vital role in the growing agriculture demand in the world. It is also a raw material for many important compounds, such as various plastics. According to the latest forecast by IFA, by 2020, the global urea production capacity will reach 229 million tons/year, and this will continue to grow [1]. Urea has the advantages of high-water solubility, low volatility, non-toxic ideal energy density, and high hydrogen content [2]. In addition, the energy density of urea is higher than liquid hydrogen; thus, urea is also regarded as a promising H<sub>2</sub> carrier. Therefore, the low-carbon process for urea production has become a research hotspot.

The main industrial route for urea production is initially producing ammonia and carbon dioxide from fossil energy (e.g., coal- and natural gas-based). As one of the main raw

materials for synthesizing urea production, more than 80% of ammonia is used as nitrogen fertilizer [3]. Nearly all commercial production of ammonia is based on the Haber–Bosch synthesis process through the synthesis of  $N_2$  and  $H_2$  ( $N_2/H_2 = 1/3$ ) at 450–600 °C and 10–250 bar [4]. The hydrogen is mainly derived from coal, natural gas, and other fossil fuels. The production of  $H_2$  mainly relies on coal and coke, and about 97% of  $H_2$  comes from these two feedstocks [5]. For the coal-to-hydrogen process, coal reacts with  $O_2$  to produce crude syngas, and after scrubbing and waste heat recovery, the crude syngas is delivered into the water–gas shift unit (WGS), in which CO and  $H_2O$  are converted to  $CO_2$  and  $H_2$ . Thus, a large amount of  $CO_2$  is generated in WGS [6,7]. In order to avoid the toxic catalyst of  $NH_3$  synthesis,  $CO_2$  is split from the  $H_2$ -rich steam in the acid gas removal unit (AGR). The AGR is a high operational cost unit mainly because a larger amount of energy is consumed.

According to the literature review, the chemical looping hydrogen (CLH) technology developed from chemical looping combustion (CLC) has tremendous potential for converting fuel into hydrogen production [8]. In this method,  $CO_2$  and  $H_2$  are generated in different reactors, which illustrates that purified  $CO_2$  and  $H_2$  are obtained relatively more easily than traditional AGR through gas–solid separation and condensation procedures. It is indicated that the energy consumption for  $CO_2/H_2$  separation is decreased obviously [9–11]. Many studies have explored that the CLH technology as a competitive method was used for low-carbon and clean hydrogen production. Ohio State University (OSU) developed and studied two looping processes: the syngas chemical looping (SCL) and the coal direct chemical looping (CDCL) technologies. The combined SCL and CDCL were continuously operated for more than 850 h, and the hydrogen with a purity of more than 99.99% and a carbon capture ratio of 100% were obtained [12]. Edrisi et al. [13] investigated an iron-based oxygen carrier chemical looping technique to convert methane and air into  $CO_2$ ,  $N_2$ , and  $H_2$ . Recently, Edrisi et al. [14] used  $N_2$  and  $H_2$  produced by chemical looping technology for ammonia synthesis. The yield of ammonia products is increased by 30%, and the investment cost is significantly reduced. Mehrpooya et al. [15] developed a new process for  $H_2$  production and net electrical power output, including biomass gasification, CLC, and  $CO_2$  capture. The proposed integrated process showed excellent performance in terms of energy efficiency and environmental benefits.

Apart from the  $H_2$  production, coke-oven gas (COG) produced in coking plants is mostly used for combustion due to COG being rich in hydrogen. It leads to a lot of waste of resources and serious environmental problems [16,17]. Because coal is rich in carbon and low in hydrogen, it is attractive to co-feed with coal by introducing COG as a supplementary hydrogen source [18]. Scholars have studied the different conceptual designs of coal and COG co-feed systems. Hao et al. [19] developed a new poly-generation system based on coal and COG co-feed for the co-production of dimethyl ether (DME)/methanol and electricity. The system performed better than the traditional  $CH_4/CO_2$  dry reforming process in terms of exergy efficiency and  $CO_2$  emission. Li et al. [20] also developed a methanol and power generation cogeneration system based on coal gasification and COG, which coupled with  $CO_2$  capture process. The results showed that the energy saving was increased by over 5%, while the exergy efficiency increased by about 50%.

The  $N_2$  required for ammonia production is obtained through air separation (AS) technology. Large-scale  $O_2$  production plants commonly use cryogenic air separation (CAS). However, CAS is characterized by high energy consumption; it is reported that the specific energy of  $O_2$  production (95% vol.%) is 200 kWh/t [21]. To seek a more economical and energy-saving  $O_2$  production process, a potentially promising technology, chemical looping air separation (CLAS) technology, has gradually attracted the attention of scholars. It is a kind of oxygen absorption and oxygen release reaction in different reactors to achieve pure oxygen production [22]. Due to its simple process, the equipment investment cost is lower than that of traditional CAS. In addition, the heat-absorbing of metal oxides is mostly provided by the heat-releasing of exothermic metal oxidation; thus, the operational cost of CLAS is decreased obviously [23]. Newcastle university concluded that CLAS

technology has great potential to replace traditional CAS through a series of experiments and modeling studies on CLAS technologies [24]. Shi et al. [25] studied a novel CLAS system and analyzed the technical/economic performance of different oxygen carriers, and the results showed that Mn-based CLAS can significantly increase the energy efficiency of the oxidation reaction and reduce the size of the reactor under specific oxidation conditions. Zhu et al. [26] investigated coal gasification integrated with CLAS; the key parameters were optimized and exergy efficiency was analyzed. The results showed that the largest exergy destroyer in the process is located in gasifier, which accounts for 65.06% of the total exergy destruction.

Although stacks of research have been produced on chemical looping technology and COG-assisted coal co-feed production for chemical production in the past few decades, to our knowledge, there have been few studies on integrating chemical looping technology and COG in the production of urea processes. On the one hand, CLH technology only using coal as a raw material does not improve carbon utilization efficiency, resulting in the waste of carbon resources [27]. On the other hand, the CLH process with COG as feedstock also results in relatively low energy efficiency due to the high hydrogen content of the COG [28]. Aiming at the above problems, a COG pressure swing adsorption (PSA)-assisted coal combined with CLAS and CLH technologies for urea production (COG-CTU<sub>CLAS&H</sub>) is proposed in this paper. The H<sub>2</sub> in the COG is separated by PSA technology, and the remaining hydrogen-poor COG is used mixed with syngas from coal gasified gas (CG) as fuel for the CLH, while the N<sub>2</sub> separated by CLAS provides the nitrogen source for the synthesis of urea. COG-CTU<sub>CLAS&H</sub> technology can efficiently produce H<sub>2</sub> and N<sub>2</sub>, which can improve the carbon utilization efficiency of raw materials and reduce CO<sub>2</sub> emissions. The operational parameters of the COG-CTU<sub>CLAS&H</sub> process are analyzed based on rigorous simulation for each unit using Aspen Plus software. The technical/economic performance of three processes (CTU, CTU<sub>CLAS&H</sub>, and COG-CTU<sub>CLAS&H</sub>) is conducted to verify the feasibility of the novel processes.

The rest of the paper is organized as follows: the CTU, CTU<sub>CLAS&H</sub>, and COG-CTU<sub>CLAS&H</sub> are described in Section 2. Section 3 is the methodology of technical performance and economic performance, including carbon utilization efficiency, energy efficiency, total capital investment, total production cost, and internal rate of return. Section 4 is the results and discussion, where the key operational parameters of the COG-CTU<sub>CLAS&H</sub> process are optimized to improve the system energy efficiency, and the technical and economic performance are analyzed. Conclusions are drawn in Section 5.

## 2. Scheme Design and Modeling

Conventional CTU mainly includes a cryogenic air separation unit (CAS), coal gasification unit (CGU), water–gas shift unit (WGS), acid gas removal unit (AGR), ammonia production unit (AP), and urea production unit (UP), as shown in Figure 1. The pulverized coal obtained from the raw coal after grinding and drying is mixed with water to make coal water slurry. The coal water slurry enters the gasifier and reacts with oxygen from the CAS to generate crude syngas. The crude syngas enters the WGS after acid hydrogen sulfide removal from the AGR, in which CO in syngas is converted into H<sub>2</sub> required for ammonia production, and a large amount of CO<sub>2</sub> is produced at the same time. The mixed gas from the WGS enters CO<sub>2</sub> capture unit, where CO<sub>2</sub> is separated by Rectisol technology and CO<sub>2</sub> is used as the carbon source for urea production. The purified gas from the CO<sub>2</sub> capture unit is further washed with liquid nitrogen to obtain pure H<sub>2</sub>. The N<sub>2</sub> from the ASU is firstly mixed with H<sub>2</sub> and then compressed and delivered to AP. The NH<sub>3</sub> and the CO<sub>2</sub> separated from the previous unit are mixed and then entered into the UP for urea production.

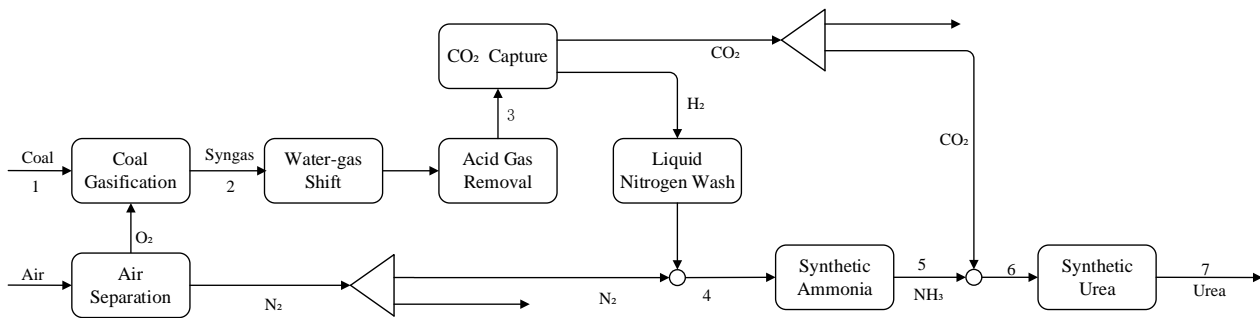


**Figure 1.** Flow diagram of conventional CTU.

The flow diagram of the  $CTU_{CLAS\&H}$  process is shown in Figure 2. The  $CTU_{CLAS\&H}$  mainly includes CGU, AGR, CLAS, CLH, AP, and UP. Compared with the conventional CTU, the  $CTU_{CLAS\&H}$  adopts advanced chemical looping technology for ammonia and urea production. In the  $CTU_{CLAS\&H}$ , the CLAS replaces the conventional CAS to produce  $O_2$  and  $N_2$  with low energy consumption. In addition, the CLH replaces the conventional WGS to produce  $H_2$ , and high-purity  $CO_2$  is obtained for synthetic urea. The CLH contains three reactors, a fuel reactor (FR), steam reactor (SR), and air reactor (AR). After desulfurization, the crude syngas enters the FR, reacts with oxygen carrier  $Fe_2O_3$ , and produces a large amount of  $CO_2$  and  $H_2O$ ; at the same time, the  $Fe_2O_3$  is broken apart into Fe and FeO, which are introduced into the SR to react with steam for  $H_2$  production, and the Fe and FeO are converted into  $Fe_3O_4$ . The  $Fe_3O_4$  from the SR enters the AR and is further oxidized to  $Fe_2O_3$ , realizing the circulation of the oxygen carrier. In the CLH, the gas and oxygen carrier can be separated by simple gas–solid separation, and  $CO_2$  and  $H_2$  are not in direct contact, which minimizes the energy consumption of gas separation and purification.

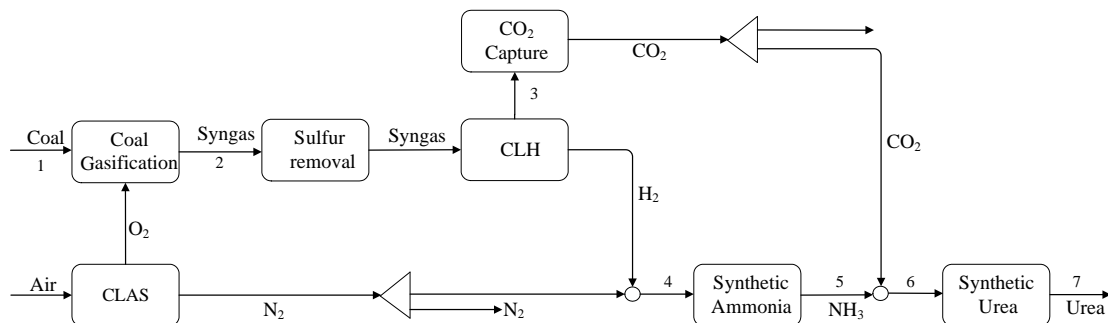


**Figure 2.** Flow diagram of  $CTU_{CLAS\&H}$ .

The flow diagram of the COG- $CTU_{CLAS\&H}$  process is shown in Figure 3. The difference between COG- $CTU_{CLAS\&H}$  and  $CTU_{CLAS\&H}$  is that coke-oven gas (COG) is introduced to produce hydrogen by pressure swing adsorption (PSA) technology in the COG- $CTU_{CLAS\&H}$ . The separated hydrogen adds a new direct  $H_2$  source for ammonia production, while the remaining hydrogen-poor coke oven gas and syngas from coal gasification are mixed and fed into the CLH to produce hydrogen, which indirectly increases the  $H_2$  source for ammonia synthesis. The increasing ammonia production improves the capacity of  $CO_2$  for urea production. The introduction of COG in the  $CTU_{CLAS\&H}$  can realize the effective utilization of COG and generate more ammonia and urea production. In addition, the carbon utilization rate and economic benefits of the whole process are effectively improved compared with the CTU and  $CTU_{CLAS\&H}$ .

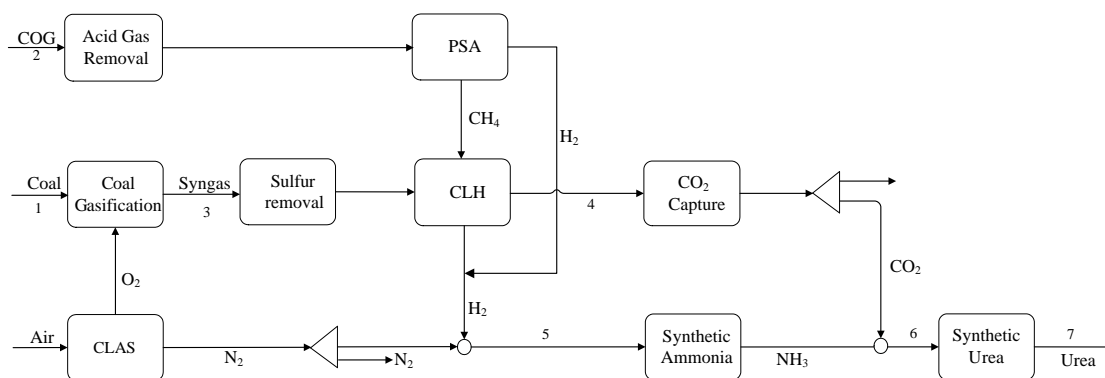


Figure 3. Flow diagram of COG-CTU<sub>CLAS&H</sub>.

### 2.1. Coal Gasification Unit

The process flowsheet of gasification is presented in Figure 4. The coal gasification process mainly includes coal water slurry preparation, gasification, waste heat recovery, and washing. In the preparation stage of coal water slurry, the raw coal is first crushed and pulverized and then mixed with water to obtain coal water slurry with coal to water ratio of 65% [29]. The Texaco coal-water slurry gasification technology is adopted. The coal slurry and O<sub>2</sub> from CLASU enter the gasifier, where the water is rapidly vaporized and the partial combustion and devolatilization reactions begin to occur simultaneously. The generated crude syngas is cooled by water quenching method using the HeatX module to recover waste heat. After water quenching, the crude syngas enters the scrubber (flash model) to remove the soluble gas, and the crude syngas is further cooled and finally sent to the sulfur removal unit.

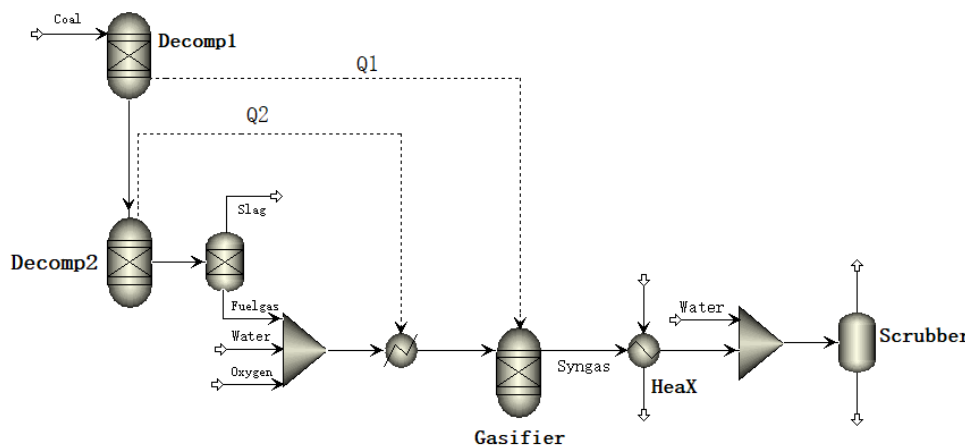
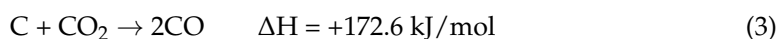
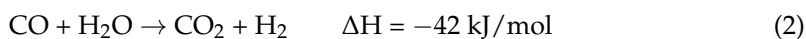
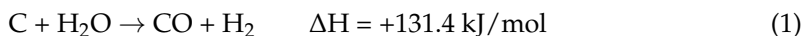
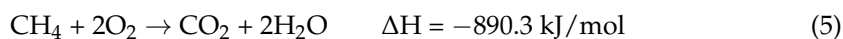


Figure 4. Process flowsheet of the coal gasification unit.

During the modeling of coal gasification, two independent processes are assumed: the pyrolysis process and the gasification process. The coal pyrolysis stage is modeled by RYield reactor to decompose coal into C, H<sub>2</sub>, O<sub>2</sub>, S, and ash at a temperature of 500 °C and pressure of 6.5 MPa [30]. The gasification stage is modeled by RGibbs reactor according to Gibbs free energy minimization. In addition, the physical property method selected is Peng–Rob model [31]. The main equations of the gasification process are shown as follows [32]:





The properties of raw coal are listed in Table 1. The components in Aspen Plus are defined as unconventional components; HCOALGEN is adopted for the enthalpy model, and DCCOALIGN is adopted for the density model [27].

**Table 1.** Proximate analysis and ultimate analysis of raw coal.

	Proximate Analysis (wt.%, ad)				Elementary Analysis (wt.%, ad)				
	M	FC	V	A	C	H	O	N	S
Coal	6.1	50.01	24.71	19.18	66.31	4.43	8.5	0.76	0.82

### 2.2. Chemical Looping Air Separation Unit

The schematic diagram of the CLAS process is shown in Figure 5. The CLAS process mainly includes oxidation reactor (OR) and reduction reactor (RR). Firstly, air is compressed by a compressor and heated up to reaction temperature; then, air is fed into the OR (RGibbs model), where  $\text{Mn}_3\text{O}_4$  is converted to  $\text{Mn}_2\text{O}_3$  by reacting with  $\text{O}_2$ , as shown in Equation (6). The reaction product out of the OR enters the separator to separate oxygen-lean air and  $\text{Mn}_2\text{O}_3$ , and oxygen-lean air is used to provide  $\text{N}_2$  for the  $\text{NH}_3$  synthesis unit. In the RR, due to the low partial pressure of oxygen, steam needs to be introduced to promote the production of  $\text{Mn}_3\text{O}_4$ , and oxygen is by-produced in this process, as shown in Equation (7);  $\text{Mn}_3\text{O}_4$  is then cycled back to the OR again. The  $\text{O}_2$  and steam out of the RR enter the separation unit, pure  $\text{O}_2$  is obtained, and  $\text{O}_2$  is required for coal gasification.

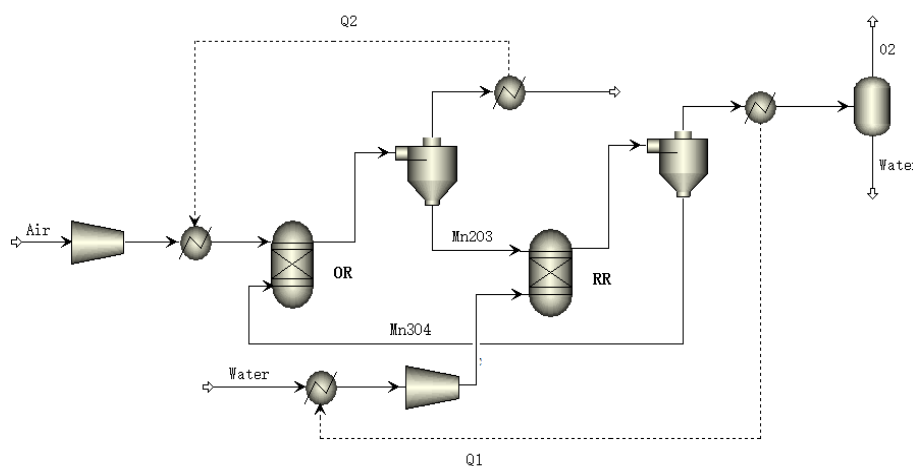
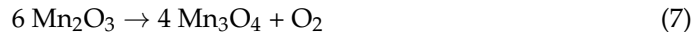


**Figure 5.** Process flowsheet of the chemical looping air separation unit.

### 2.3. Chemical Looping Hydrogen Unit

The main units of CLH process include a fuel reactor (FR), steam reactor (SR), and air reactor (AR). The circulating oxygen carrier (OC) is  $\text{Fe}_2\text{O}_3$  with the inert material  $\text{MgAl}_2\text{O}_4$  (70% wt.).  $\text{Fe}_2\text{O}_3$  is selected because  $\text{Fe}_2\text{O}_3$  has the advantages of being cheap and having high reactivity; moreover,  $\text{Fe}_2\text{O}_3$  makes the water vapor has a high conversion rate [33–35]. Inert materials are used to control the temperature of the solids and reduce heat stress. In these sub-processes, the thermodynamic method of Peng–Rob is used for simulation.

Figure 6 depicts a flowsheet of the CLH process. After washing, desulfurization, and compression, the syngas enters the CLH process. The purified syngas is almost completely oxidized to  $\text{CO}_2$  and  $\text{H}_2\text{O}$  by  $\text{Fe}_2\text{O}_3$  in the FR (RGibbs model), and gas–solid separation is performed using a cyclone separator (Cyclone model). In this work, gas–solid separation is

assumed to be complete. After gas–solid separation, the gas phase passes heat exchange and is fed into the flash tank to separate the steam and CO<sub>2</sub>. The reduced oxygen carrier enters the SR (RGibbs model), where Fe, FeO, and the steam react to form a mixture of H<sub>2</sub>. Fe<sub>3</sub>O<sub>4</sub> is separated from H<sub>2</sub> and steam through the cyclone separator, and the gas phase is transported by the compressor to the flash tank after the heat exchanger, and the hydrogen is separated from the steam to obtain high-purity H<sub>2</sub>. Fe<sub>3</sub>O<sub>4</sub> enters the air reactor (AR) and reacts with O<sub>2</sub> in the air with a strongly exothermic reaction. After the gas–solid separation by the cyclone separator, the high-temperature and high-pressure hypoxic air enters the waste heat boiler (HeatX model) to recover the heat, and the solid oxygen carrier circulates into the combustion reactor (FR).

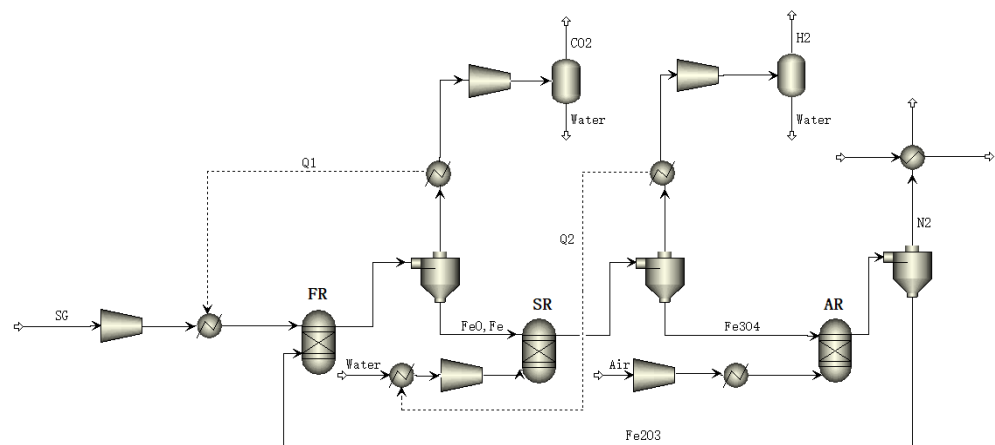
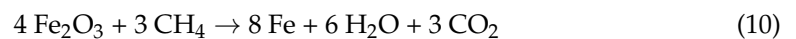
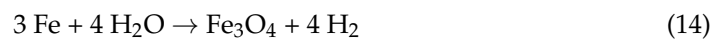


**Figure 6.** Process flowsheet of the chemical looping hydrogen unit.

The reactions occurring in the FR are shown in Equations (8)–(12):



The reactions occurring in the SR are shown in Equations (13) and (14):



The reactions occurring in the AR are shown in Equation (15):



#### 2.4. Ammonia Synthesis Unit

The flowsheet of the ammonia synthesis unit is shown as Figure 7. It mainly includes feed gas pretreatment, reaction, and purification parts. In the raw gas pretreatment stage, H<sub>2</sub> and N<sub>2</sub> are compressed and pressurized by the compressor and enter the catalytic oxidation reactor (Requil model); after removing a small amount of O<sub>2</sub>, the molar ratio of H<sub>2</sub> and N<sub>2</sub> is about 3, and they are then delivered into the dryer (Flash model). After removing the H<sub>2</sub>O in the mixed gas, the purified raw material gas passes and is compressed and enters ammonia synthesis reactors after passing through the heat exchanger. Since the synthesis ammonia reaction is exothermic, R1 can exchange heat with the feed N<sub>2</sub>, R2

pre-heats the cold feed, and the unreacted gas at the R3 outlet is mixed with the preheated feed. After the purified part of the unreacted gas and NH<sub>3</sub> are further cooled by the heat exchanger into the flash tank (Flash model).

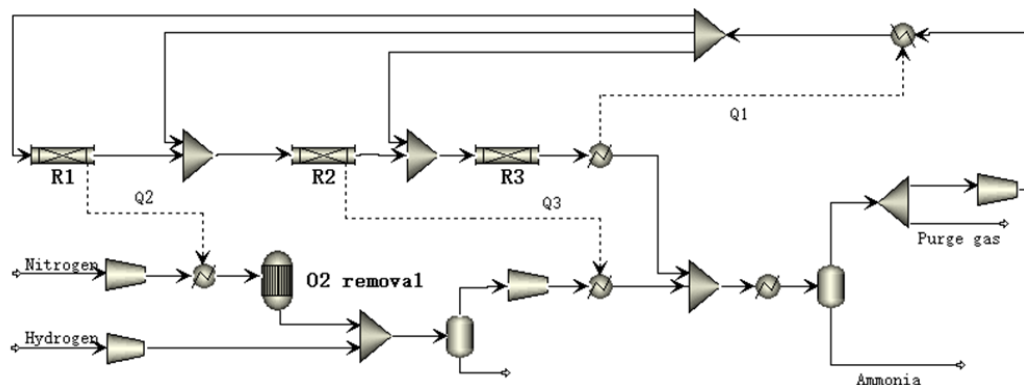


Figure 7. Process flowsheet of the ammonia synthesis unit.

The ammonia production is achieved in liquid flow, while the gas flow contains a large amount of unreacted gas, of which a small amount is discharged as a purge gas, and the remaining gas enters the reaction part of the cycle. The Rplug block is used to model the NH<sub>3</sub> reactor and main reaction equation is shown in Equation (16). The kinetic rate equation, Equation (17), can be found in Morud et al. [36] and Flórez-Orrego et al. [37], and additional detailed parameters for the optimization of ammonia synthesis can be found in Xiang et al. [38] and Araújo et al. [39].



$$r_{\text{NH}_3} = \frac{2f}{\rho_{\text{cat}}} \left( k_1 \frac{P_{\text{N}_2} P_{\text{H}_2}^{1.5}}{P_{\text{NH}_3}} - k_{-1} \frac{P_{\text{NH}_3}}{P_{\text{H}_2}^{1.5}} \right) \quad (17)$$

where  $P$  represents the partial pressure;  $\rho_{\text{cat}}$  represents the catalyst density;  $f$  is the correction factor, 4.75;  $k_1$  and  $k_{-1}$  represent the pre-exponential factors:  $k_1 = 1.79 \times 104e^{-10,475/T}$ ,  $k_{-1} = 2.75 \times 1016e^{-23,871/T}$ ; and  $T$  represents the temperature (K).

### 2.5. Urea Synthesis Unit

Commercial urea synthesis is based on the Basarov reaction [40] (Equations (18) and (19)) at 125–250 bar and 170–220 °C, according to the following two reactions:



The urea synthesis adopts a mature CO<sub>2</sub> stripping process (Figure 8). A large amount of ammonium carbamate produced in the urea reactor enters the CO<sub>2</sub> stripping tower (RadFrac model) and decomposes into NH<sub>3</sub> and CO<sub>2</sub>. NH<sub>3</sub> and CO<sub>2</sub> circulate into the urea reactor, and the liquid stream from the bottom of the CO<sub>2</sub> stripping tower is rich in urea and enters the urea purification unit; in the urea synthesis part, NH<sub>3</sub> is mixed with the circulating gas and delivered into a high-pressure condenser (RStoic model) to react with NH<sub>3</sub> to generate ammonium carbamate and is then fed into the urea synthesis reactor (Rplug model), where the urea solution overflows from the bottom of the reactor to the CO<sub>2</sub> stripper, while the unreacted gas overflows from the top of the reactor into the scrubber (RadFrac model). Unreacted NH<sub>3</sub> and CO<sub>2</sub> contact with a carbamate solution recovered from the urea purification section, while gases O<sub>2</sub>, N<sub>2</sub>, and other gases are discharged from the top of the scrubber. In the purification section, the urea-rich liquid from the bottom of the CO<sub>2</sub> stripper enters the CARB decomposer (RStoic model), further decomposes the

ammonium carbamate in the liquid phase into CO<sub>2</sub> and NH<sub>3</sub>, and enters the urea separator (SEP model) to separate urea production and gas phase. The gas phase containing CO<sub>2</sub> and NH<sub>3</sub> then are fed into the CARB regenerator (RGibbs model) to produce ammonium carbamate and then enter the scrubber to absorb CO<sub>2</sub> and NH<sub>3</sub>, which eventually circulate into the synthetic urea synthesis unit.

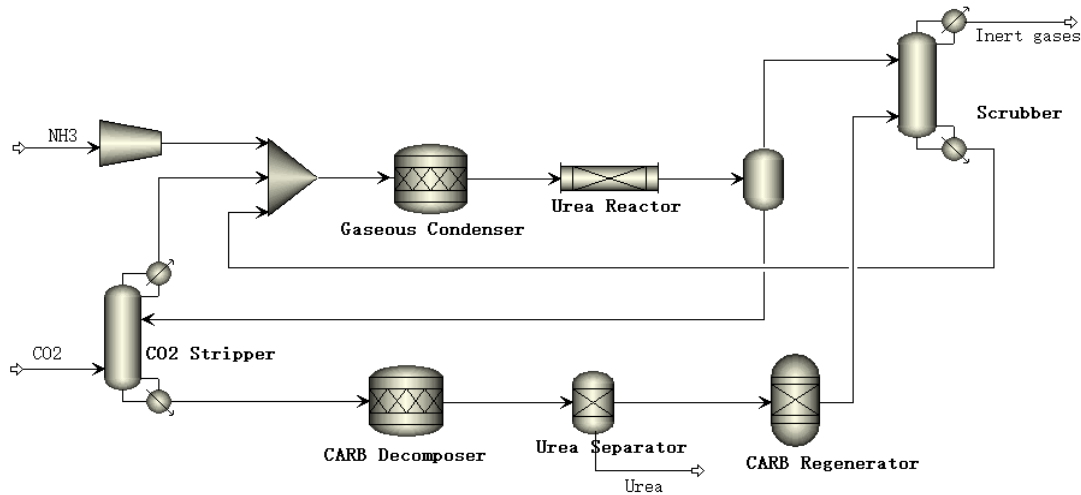


**Figure 8.** Process flowsheet of the urea synthesis unit.

### 3. Methodology

#### 3.1. Carbon Utilization Efficiency

The carbon flow analysis is an important technical indicator for the COG-CTU<sub>CLAS&H</sub> and CTU<sub>CLAS&H</sub> processes [41]. The carbon utilization efficiency and CO<sub>2</sub> emission rate are expressed in Equations (20) and (21).

$$\delta_1 = \frac{C_{\text{output}}}{C_{\text{input}}} \times 100\% = \frac{C_{\text{urea}}}{C_{\text{coal}} + C_{\text{COG}}} \times 100\% \quad (20)$$

$$\delta_2 = \frac{C_{\text{input}} - C_{\text{output}}}{C_{\text{input}}} \times 100\% = \left(1 - \frac{C_{\text{urea}}}{C_{\text{coal}} + C_{\text{COG}}}\right) \times 100\% \quad (21)$$

where  $\delta_1$  is the carbon utilization efficiency, and  $\delta_2$  is the CO<sub>2</sub> emission rate.  $C_{\text{input}}$  represents the input C in raw materials, which include coal and COG.  $C_{\text{output}}$  represents the output in the production, which is urea for the COG-CTU<sub>CLAS&H</sub> and CTU<sub>CLAS&H</sub> processes.

#### 3.2. Energy Efficiency

Energy efficiency is an important indicator for comparing the COG-CTU<sub>CLAS&H</sub> and CTU<sub>CLAS&H</sub> processes [42]. The effect of COG/CG on the utilities and energy efficiency and the energy efficiency of CTU<sub>CLAS&H</sub> and COG-CTU<sub>CLAS&H</sub> processes are shown in Equations (22) and (23), respectively. The energy consumption is calculated by Equation (24).

$$\eta_1 = \frac{E_{x,\text{out}}}{E_{x,\text{in}}} \times 100\% = \frac{E_{x,\text{urea}}}{E_{x,\text{coal}} + E_{x,\text{util}}} \times 100\% \quad (22)$$

$$\eta_2 = \frac{E_{x,\text{out}}}{E_{x,\text{in}}} \times 100\% = \frac{E_{x,\text{urea}}}{E_{x,\text{coal}} + E_{x,\text{COG}} + E_{x,\text{util}}} \times 100\% \quad (23)$$

$$E_{x,\text{util}} = E_{x,\text{steam}} + E_{x,\text{ele}} \quad (24)$$

where  $\eta_1$  and  $\eta_2$  represent the system energy efficiencies of the CTU<sub>CLAS&H</sub> and COG-CTU<sub>CLAS&H</sub> processes.  $E_{x,\text{out}}$  and  $E_{x,\text{in}}$  represent the output and input energy,  $E_{x,\text{coal}}$ ,  $E_{x,\text{COG}}$ ,

and  $E_{x,util}$  represent the energy of coal, COG, and utilities, respectively.  $E_{x,stream}$  and  $E_{x,ele}$  represent the energy of stream and electricity.

### 3.3. Total Capital Investment

The total capital investment (TCI) consists of fixed capital investment and working capital. The fixed capital investment mainly includes the direct investment and indirect investment which correspond to the costs of equipment, installation, engineering, supervision, etc. The equipment cost ( $I_{EI}$ ) is generally the most important component of the TCI and the rest costs of TCI have a ratio to equipment cost. We adopt the plant capacity index method to calculate the equipment cost, as shown in Equation (25), and TCI is calculated according to Equation (26) [42,43].

$$I_{EI} = I_{EI}^{ref} \times \theta \times \left( \frac{S}{S_{ref}} \right)^{sf} \quad (25)$$

$$TCI = I_{EI} \times \sum (1 + \zeta_i) \quad (26)$$

where  $I_{EI}^{ref}$  and  $S_{ref}$  are the equipment investment and processing scale of the present plants.  $\theta$  is the domestic production index with 0.65, and  $sf$  is the scale index with 0.67.  $\zeta_i$  is the ratio of other costs in TCI to equipment cost, as shown in Table S1.

### 3.4. Total Production Cost

We investigate the total product costs (TPC) of the CTU, CTU<sub>CLAS&H</sub>, and COG-CTU<sub>CLAS&H</sub> to compare the economic performance of all three processes. The product costs are calculated by referring to our previous works as shown in Equation (27) [31,44]. In order to calculate the product costs, the following assumptions are made: the prices of coal, COG, stream, electricity and urea are USD 100/t, USD 0.06/m<sup>3</sup>, USD 6.0/GJ, USD 0.1/kW·h, and USD 357.14/t, respectively. The assumptions for 15 years of depreciation and a residual value of 4% were used for calculating the depreciation cost [42]. The exchange rate between the US dollar and the Chinese yuan is set at 7.0 yuan per US dollar.

$$TPC = C_r + C_u + C_{om} + C_d + C_{poc} + C_{ge} \quad (27)$$

where  $C_r$ ,  $C_u$ ,  $C_{om}$ ,  $C_d$ ,  $C_{poc}$ , and  $C_{ge}$  represent costs of raw material, utilities, operation and maintenance, depreciation, plant overhead, and general expenses, respectively. Detailed calculation data are shown in Table S2.

### 3.5. Internal Rate of Return

To assess the feasibility of the CTU<sub>CLAS&H</sub> and COG-CTU<sub>CLAS&H</sub> processes, the internal rate of return (IRR) is investigated in this work. It can be defined as the discount rate ( $i$ ) at which the net present value equals to zero, given by [38]:

$$\sum_{t=0}^n \frac{NCF_t}{(1+i)^t} = 0, \quad (28)$$

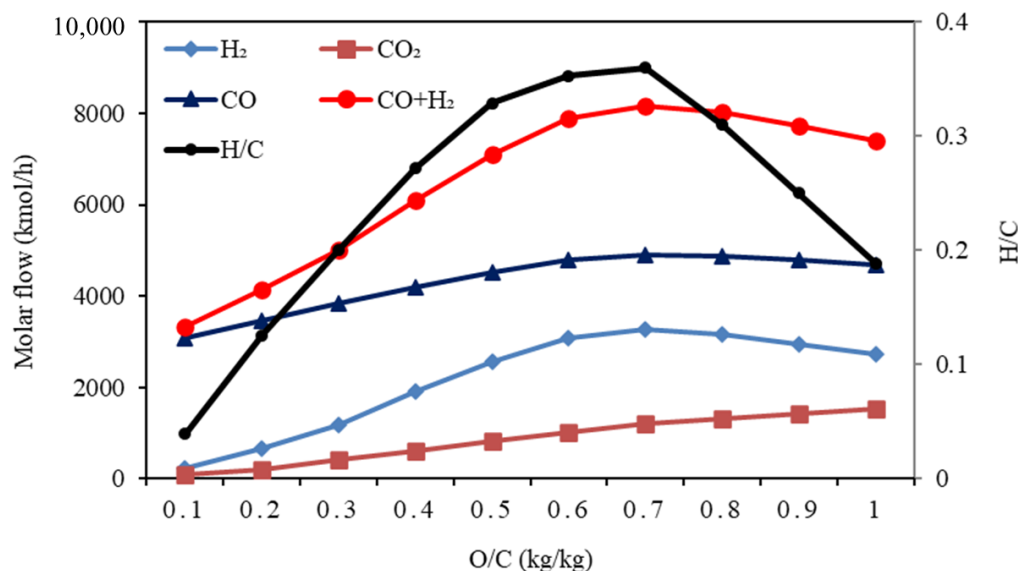
where  $NCF$  and  $n$  are the net cash flow and project life period, respectively.

## 4. Results and Discussion

### 4.1. Parameter Optimization and Simulation

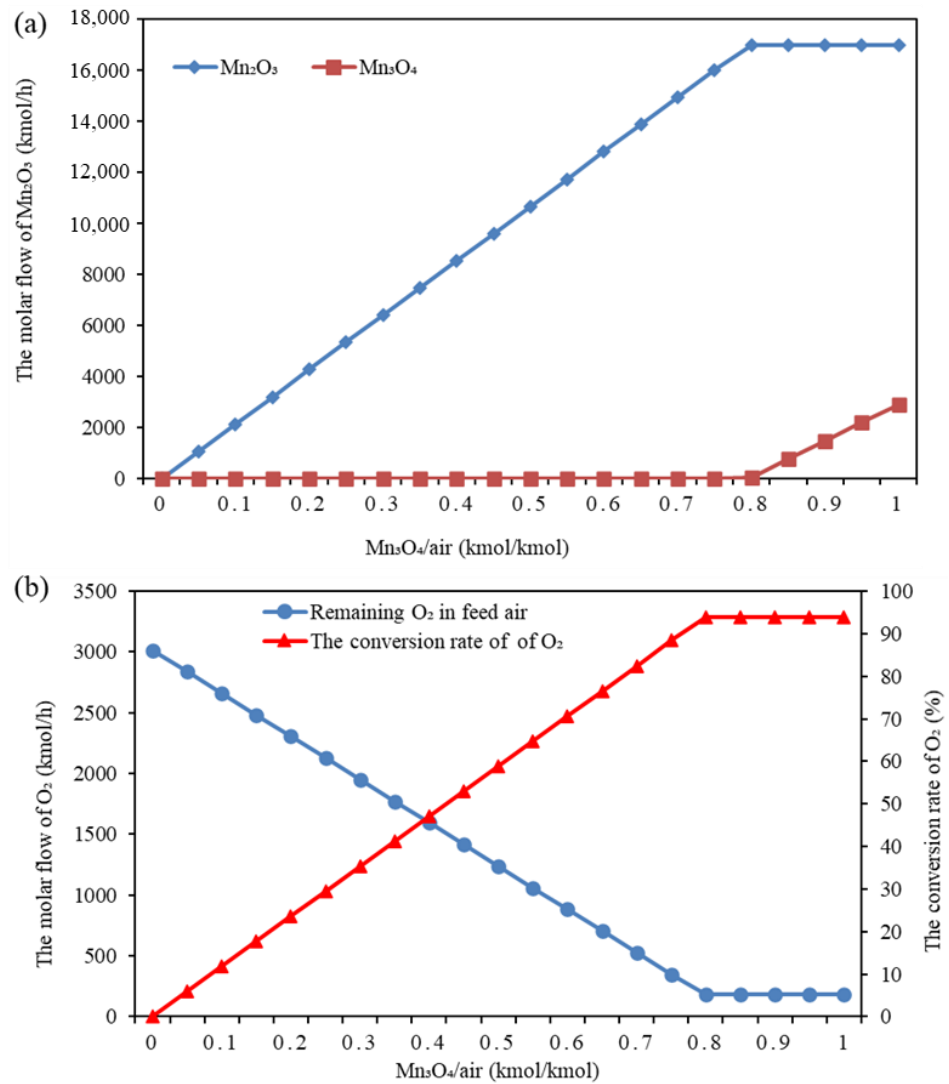
To increase the yield of urea production and the conversion of raw material as well as the techno-economic performance of the novel process, several key parameters of the process are investigated and optimized in the following section, including oxygen/coal ratio (O/C ratio) in the coal gasification,  $Mn_3O_4$ /air and stream/ $Mn_2O_3$  in the CLAS, and  $Fe_2O_3$ /CG and stream flow rate in the CLH.

The O/C ratio is an important parameter for coal gasification due to the O/C ratio significantly affecting the flow and composition of produced crude synthesis. The effects of the O/C ratio on the gasifier performance (molar flow and H/C of crude syngas) are shown in Figure 9. In the range of 0.1–1.0, the molar flow of the components ( $H_2 + CO$ ) first increases as the O/C ratio increases and reaches the highest level (8158.88 kmol/h) when the O/C ratio is 0.7 and 0.31 is obtained for the H/C ratio. When the O/C ratio increases from 0.7 to 0.9, the molar flow rate ( $CO + H_2$ ) shows a downward trend, while the  $CO_2$  molar flow rate shows a rising trend because the high O/C means that the oxygen content entering the gasifier increases, and more CO reacts with  $O_2$  to generate  $CO_2$  in the gasifier. Therefore, 0.7 is suggested for the O/C ratio in this work.



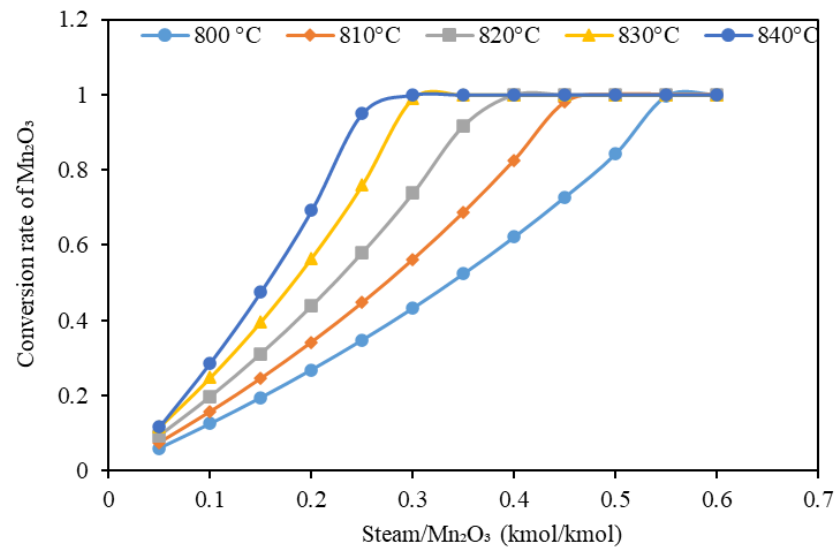
**Figure 9.** Effect of the O/C ratio on the performance of the coal gasifier.

Figure 10a emphasizes the effect of the  $Mn_3O_4$ /air ratio on the molar flow of  $Mn_3O_4$  and  $Mn_2O_3$  for the CLAS system. When  $Mn_3O_4$ /air increases from 0 to 0.8, the molar flow rate of  $Mn_2O_3$  shows a rising trend and the molar flow rate of  $Mn_3O_4$  stays at 0, which is due to the complete conversion of  $Mn_3O_4$  to  $Mn_2O_3$  under excess air.  $Mn_3O_4$ /air continues to increase to over 1, the molar flow rate of  $Mn_2O_3$  remains constant, and  $Mn_3O_4$  shows a rising trend, which is due to the oxidation reaction of  $Mn_3O_4$  with air already reaching the limit. Figure 10b indicates the effect of different  $Mn_3O_4$ /air on  $O_2$  conversion and molar flow rate of unreacted  $O_2$  in air; when  $Mn_3O_4$ /air increases from 0 to 0.8, the  $O_2$  conversion shows an increasing trend from 0 to 94%, and the corresponding molar flow rate of unreacted  $O_2$  in air shows a decreasing trend from 3016.42 kmol/h. When  $Mn_3O_4$ /air increased from 0.8 to 1, the conversion of  $O_2$  and the molar flux of unreacted  $O_2$  in air did not change, again indicating that the reaction had reached its limit when  $Mn_3O_4$ /air is 0.8. Therefore,  $Mn_3O_4$ /air is determined to be 0.8 in this paper.



**Figure 10.** Effect of the  $\text{Mn}_3\text{O}_4/\text{air}$  ratio on the molar flow (a)  $\text{Mn}_3\text{O}_4$  and  $\text{Mn}_2\text{O}_3$ , (b)  $\text{O}_2$  conversion and remaining  $\text{O}_2$  in feed air.

At the same temperature, the  $\text{Mn}_2\text{O}_3$  conversion rate increases with the increase in the stream/ $\text{Mn}_2\text{O}_3$  ( $S/\text{Mn}_2\text{O}_3$ ) ratio. Under the same  $S/\text{Mn}_2\text{O}_3$  ratio, the higher conversion rate of the  $\text{Mn}_2\text{O}_3$  is achieved with increase in the reaction temperature, indicating that increasing the reduction temperature within a certain range can promote the reduction reaction. As the temperature changes from 800 to 840 °C, the steam/ $\text{Mn}_2\text{O}_3$  ratio changes from 0.25 to 0.6 to maintain the  $\text{Mn}_2\text{O}_3$  conversion at 95%. When the temperature is 830 °C and  $S/\text{Mn}_2\text{O}_3$  is 0.3, the  $\text{Mn}_2\text{O}_3$  conversion rate can reach 100%. In order to realize 100% of the  $\text{Mn}_2\text{O}_3$  conversion and lower steam consumption, 830 °C and 0.3 are chosen for reaction temperature and  $S/\text{Mn}_2\text{O}_3$  ratio, respectively, as shown in Figure 11.



**Figure 11.** Effect of the S/Mn<sub>2</sub>O<sub>3</sub> on the Mn<sub>2</sub>O<sub>3</sub> conversion at different reduction temperatures.

Figure 12 shows the effect of the Fe<sub>2</sub>O<sub>3</sub>/CG on the molar flow rate. When Fe<sub>2</sub>O<sub>3</sub>/CG increases from 0 to 0.3, the molar flow rate of H<sub>2</sub> and CO decreases with the increase in Fe<sub>2</sub>O<sub>3</sub>/CG. When Fe<sub>2</sub>O<sub>3</sub>/CG increases from 0.3 to 0.5, the molar flow rate of H<sub>2</sub> and CO almost completely reacts with CO<sub>2</sub>. The molar flow rate of Fe increases with the increase in Fe<sub>2</sub>O<sub>3</sub>/CG. When Fe<sub>2</sub>O<sub>3</sub>/CG increases from 0.3 to 0.5, the molar flow rate of CO<sub>2</sub> and Fe does not change. This is because when Fe<sub>2</sub>O<sub>3</sub>/CG is 0.3, the molar flow rate of H<sub>2</sub> and CO in the reactor is very low, and the reaction reaches the limit. In this analysis, the molar flow rate of FeO is very low in the case of excessive syngas. According to Equation (14), the higher the molar flow rate of Fe is, the more favorable it is for H<sub>2</sub> generation. Therefore, Fe<sub>2</sub>O<sub>3</sub>/CG is chosen as 0.3.

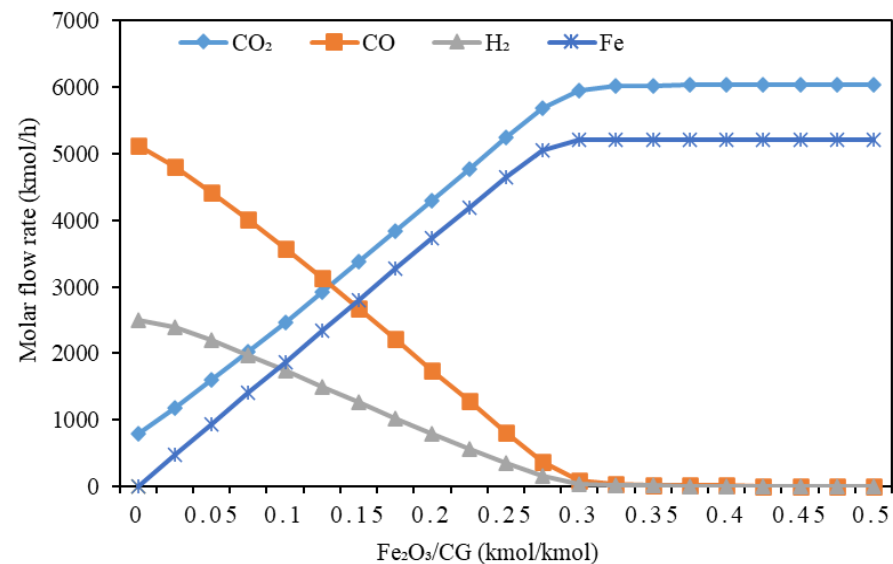


**Figure 12.** Effect of the Fe<sub>2</sub>O<sub>3</sub>/CG on the molar flow rate of the CTU<sub>CLAS&H</sub> process.

Figure 13 shows the effect of the steam on the Fe<sub>3</sub>O<sub>4</sub> and H<sub>2</sub> molar flow rate and the Fe conversion rate. When the molar flow rate of water vapor is from 0 to 8250 kmol/h, the molar flow rate of Fe<sub>3</sub>O<sub>4</sub> and the molar flow rate of Fe conversion H<sub>2</sub> show an upward trend. However, when the molar flow rate of water vapor continues to increase, the Fe<sub>3</sub>O<sub>4</sub> generation rate changes very little, indicating that the reaction has tended to reach its limit.

At this time, the molar flow rate of hydrogen reaches 6836.79 kmol/h, and the conversion rate of Fe reaches 97%. The remaining Fe is completely oxidized to  $\text{Fe}_2\text{O}_3$  in the AR reactor.

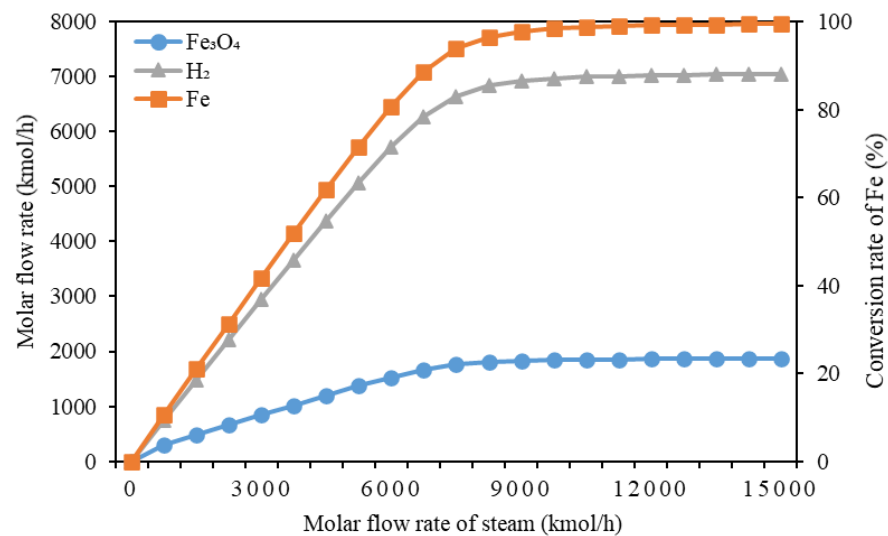


**Figure 13.** Effect of the steam on the  $\text{Fe}_3\text{O}_4$  and  $\text{H}_2$  molar flow rate and the Fe conversion rate.

The efficiency of the process model and simulation can be verified by comparing the calculation and reference results. The simulation agrees well with the reference data, as shown in Table 2. Detailed simulation results are shown in Tables S3–S5 in the Supporting Materials.

**Table 2.** Comparison of the simulation and reference data.

CLHU	Ref.	Sim.	Unit	Ref.
<b>FR parameters</b>				
Heat duty	0.0	0.0	MW	[45]
CO purity	~0.0	~0.0	Mol. %	
$\text{Fe}_2\text{O}_3$ conversion	100	100	%	
<b>SR parameters</b>				
Operating temperature	700–750	700	$^{\circ}\text{C}$	[13]
Heat duty	0.0	0.0	MW	
Steam conversion	30–50	58.5	%	
<b>AR parameters</b>				
Operating temperature	1200	1200	$^{\circ}\text{C}$	[13]
$\text{Fe}_3\text{O}_4$ conversion	100	100	%	
$\text{N}_2$ purity	99.8	99.7	99.7	
Operating pressure	1.0	1.0	MPa	
<b>CLAS</b>				
<b>OR parameters</b>				
Operating pressure	Ambient	Ambient	-	[26]
$\text{Mn}_2\text{O}_3$ conversion	100	100	%	
<b>XR parameters</b>				
Operating temperature	800–900	830	$^{\circ}\text{C}$	[26]
Operating pressure	1	1	bar	
$\text{Mn}_3\text{O}_4$ conversion	100	100	%	

Table 2. Cont.

CLHU	Ref.		Sim.		Unit	Ref.
APU	Input	Output	Input	Output		[28]
H <sub>2</sub> purity	75.0	2.2	74.8	1.2	mol.%	
N <sub>2</sub> purity	25.0	0.8	25.2	0.3	mol.%	
NH <sub>4</sub> purity	-	97.0		98.2	mol.%	
Operating temperature	723–729		731–738		K	
Operating pressure	20.1–20.3		20.1–20.3		MPa	

#### 4.2. Technical Performance Analysis

##### 4.2.1. Carbon Utilization Efficiency Analysis

Figure 14 investigates the effect COG/CG on the carbon utilization efficiency and the CO<sub>2</sub> emission rate. Both carbon input and carbon output are on the rise. This is because with the increase in coke oven gas, the output of H<sub>2</sub> is directly increased, and the output of urea is also increased, while the carbon emission is on the decline. This is because more CO<sub>2</sub> is used to produce urea. With the growth of COG/CG, the carbon emission rate showed a decreasing trend, while the carbon utilization rate showed a rising trend. When COG/CG increased from 0 to 1.4, the carbon utilization rate increased from 35.67% to 81%, which proved that the introduction of coke-oven gas greatly improved the utilization of raw materials for urea production and improved the carbon utilization ratio of the traditional CTU process.

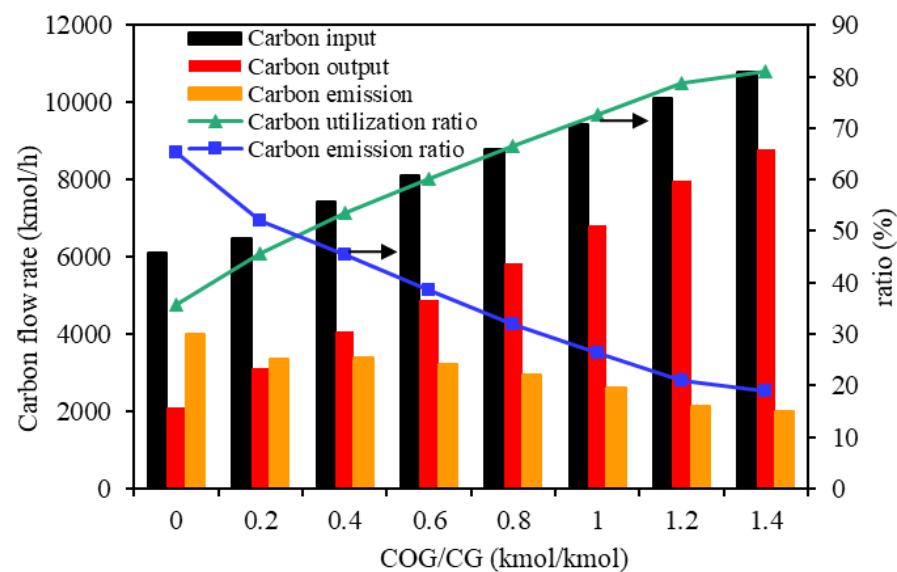
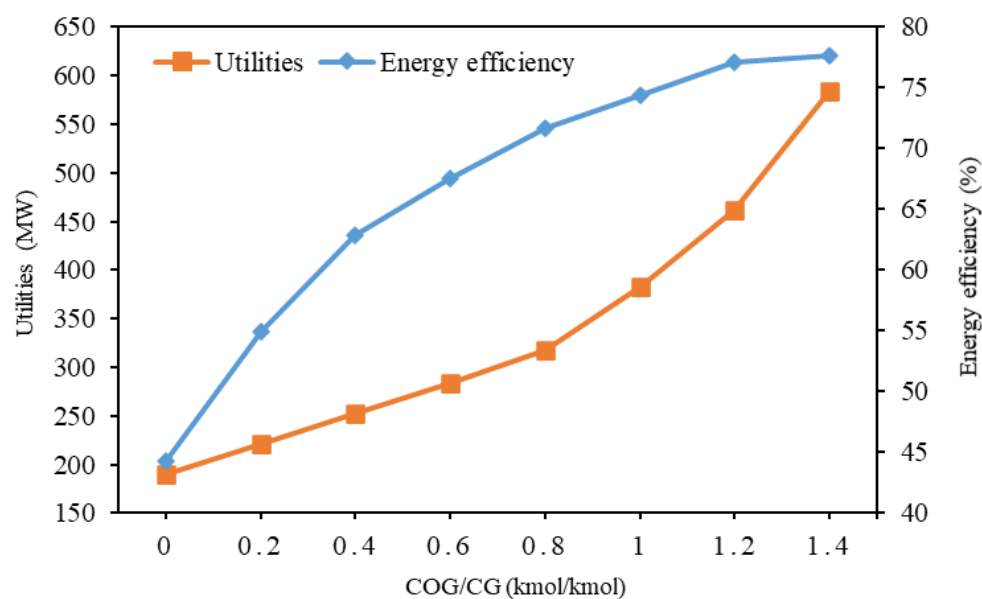


Figure 14. Effect COG/CG on the carbon utilization efficiency and the CO<sub>2</sub> emission rate.

##### 4.2.2. Energy Efficiency Analysis

The energy efficiency is analyzed in this work, as shown in Figure 15. The minimal usage of utilities is obtained when the COG/CG ratio is 0, where the system energy efficiency is also the least (44.3%). At this time, H<sub>2</sub> production in the system is insufficient, resulting in low urea production, and a large amount of CO<sub>2</sub> is not used.



**Figure 15.** Effect of COG/CG on utilities and energy efficiency.

When COG/CG rises from 0 to 1.2, utility consumption and energy efficiency increase. When COG/CG rises from 1.2 to 1.4, the increase in energy efficiency tends to be constant, which is mainly because the introduction of COG generates more  $H_2$ , which indirectly increases the yield of urea. In addition, the processing capacity of each unit increases with the increase in COG/CG, which means that the energy consumption of each piece of equipment also increases.

The above analysis shows that increasing the output of products often contributes to high energy consumption of equipment. We need to find a balance between increasing the output of products and the energy consumption of the process while taking into account the impact of the process on the environment. COG-CTU<sub>CLAS&H</sub> process can improve the production output, system energy efficiency, and carbon utilization rate. However, a high proportion of COG feedstock can increase energy consumption to the contrary. Thus, 1.2 is obtained for COG/CG value In this work.

#### 4.2.3. Technical Performance Comparison

As illustrated in Figure 16, the energy efficiency and carbon utilization rate of the CTU, CTU<sub>CLAS&H</sub>, and COG-CTU<sub>CLAS&H</sub> processes are compared. The CTU<sub>CLAS&H</sub> achieves a system efficiency of 44.30%. The CTU process only reaches an efficiency of 37.07%. This is mainly because that the energy consumption of CLHU and CLAU in CTU<sub>CLAS&H</sub> processes is lower than that of ASU and AGR in the traditional CTU process. Since the COG feedstock is required, the energy efficiency of the COG-CTU<sub>CLAS&H</sub> process can reach as high as 77.10%. For the COG-CTU<sub>CLAS&H</sub>, a significant amount of  $H_2$  is obtained by CLHU and PSA, which can be applied in  $NH_3$  synthesis to realize the increase in urea production output. Therefore, the efficiency of COG-CTU<sub>CLAS&H</sub> is enhanced by 40.03% more than that of the traditional CTU process.

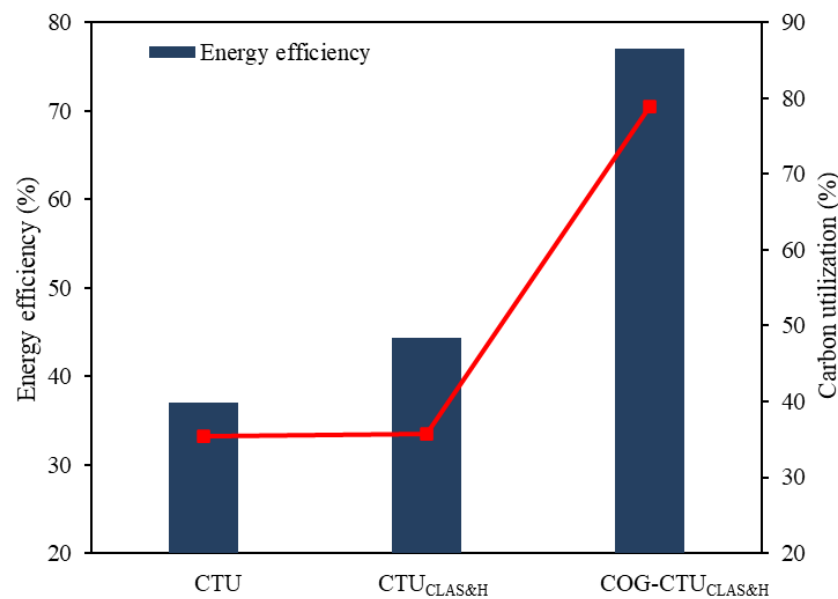


**Figure 16.** Energy and carbon utilization efficiencies of CTU, CTU<sub>CLAS&H</sub>, and COG-CTU<sub>CLAS&H</sub>.

The carbon utilization efficiency of CTU<sub>CLAS&H</sub> process is 35.67%, similar to that of the CTU process (35.42%). Carbon is mainly emitted in the form of carbon dioxide due to the low H<sub>2</sub> flow rate of CTU and CTU<sub>CLAS&H</sub>. Contrary to the CTU and CTU<sub>CLAS&H</sub>, enough H<sub>2</sub> provided by COG feedstock and CLHU ensures that almost all of CO<sub>2</sub> is converted to urea production and achieves a carbon utilization efficiency of 78.94%. Due to the high efficiency, the CO<sub>2</sub> capture scale and operating cost are remarkably lower than that of CTU and CTU<sub>CLAS&H</sub>.

#### 4.3. Economic Performance Analysis

##### 4.3.1. Total Capital Investment Analysis

According to Equations (25) and (26) and Table S1, the TCIs of the CTU, CTU<sub>CLAS&H</sub>, and COG-CTU<sub>CLAS&H</sub> are calculated and the results are shown in Figure 17. The TCI of the CTU<sub>CLAS&H</sub> is 1687.34 M\$/y, which is 18.81% lower than that of the CTU (2078.14 M\$/y). This is mainly because that the CTU<sub>CLAS&H</sub> process adopts CLAS and CLH technologies to produce oxygen and hydrogen for low energy consumption and low capital investment compared to that of the conventional CAS and WGS in the CTU process. Compared with the CTU and CTU<sub>CLAS&H</sub>, the TCI of the COG-CTU<sub>CLAS&H</sub> is increased to 2207.44 M\$/y. Because the flowsheet of the COG-CTU<sub>CLAS&H</sub> is longer than that of the CTU and CTU<sub>CLAS&H</sub>, it requires the pretreatment of COG and then pressure swing adoption for hydrogen and methane separation. The hydrogen is introduced into the AP unit and methane is introduced into the CLH unit. The processing scales of the CLH, AP, and UP units are increased as the introduction of COG. Hence, the COG-CTU<sub>CLAS&H</sub> has the largest capital cost.

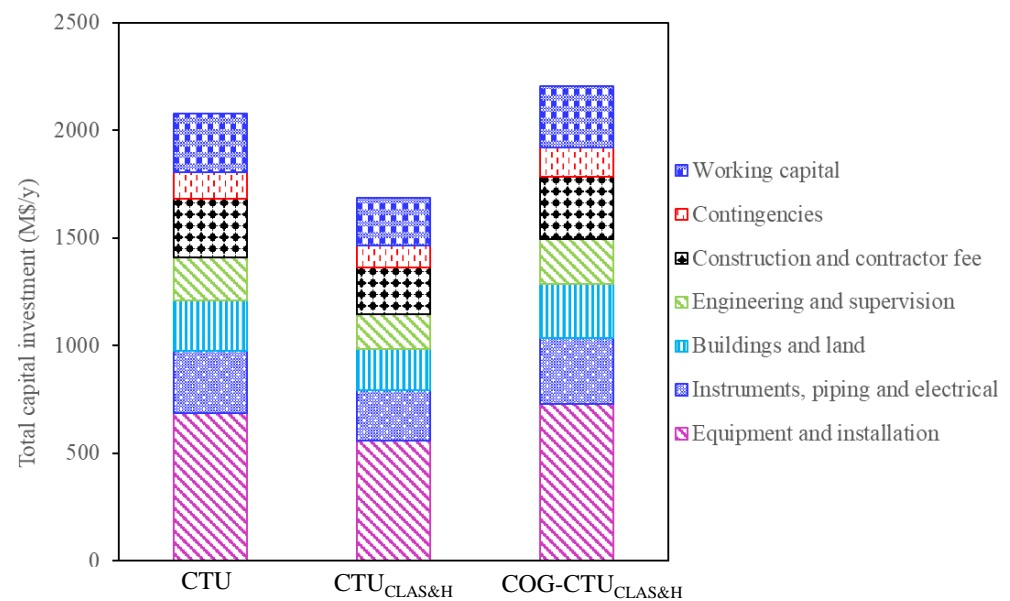


**Figure 17.** Total capital investments of CTU, CTU<sub>CLAS&H</sub> and COG-CTU<sub>CLAS&H</sub>.

#### 4.3.2. Total Production Cost Analysis

After calculation based on Equation (27) and Table S2, the TPCs of the CTU, CTU<sub>CLAS&H</sub> and COG-CTU<sub>CLAS&H</sub> are shown in Figure 18. They are USD 174.65/t-urea, USD 162.11/t-urea, and USD 201.34/t-urea, respectively. The TPC of the COG-CTU<sub>CLAS&H</sub> is 15.28% and 24.19% larger than that of the CTU and CTU<sub>CLAS&H</sub>. This is mainly because the introduction of COG of the CTU<sub>CLAS&H</sub> for high carbon utilization, which makes the raw material costs 1.56 and 1.57 times that of the CTU and CTU<sub>CLAS&H</sub>. However, the COG-CTU<sub>CLAS&H</sub> has the largest urea production, which is approximately 2.0 times that of the CTU and CTU<sub>CLAS&H</sub>. Thus, the increase in other costs, excluding raw material costs of unit urea, is not clearly comparable to that of the CTU and CTU<sub>CLAS&H</sub>.

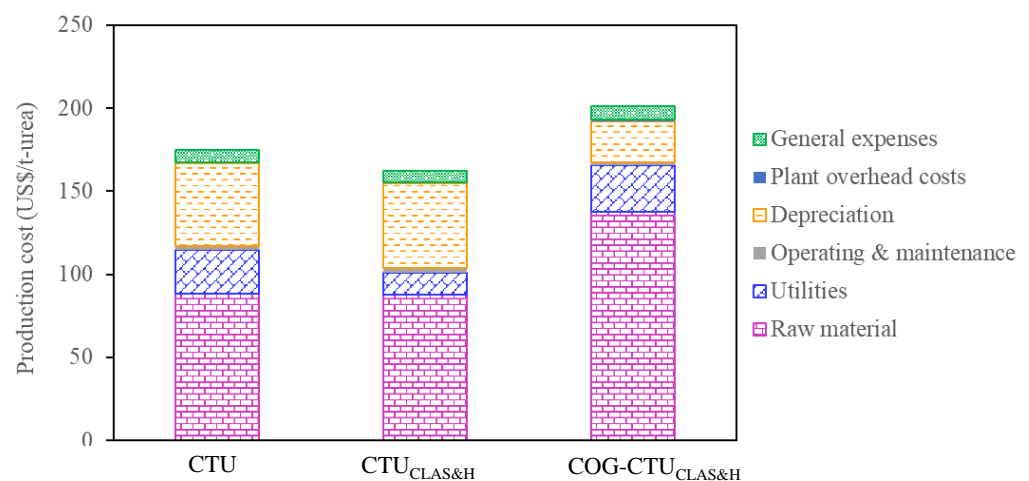


**Figure 18.** Product costs of CTU, CTU<sub>CLAS&H</sub>, and COG-CTU<sub>CLAS&H</sub>.

#### 4.3.3. Sensitivity Analysis

For the total production cost analysis, e.g., COG-CTU<sub>CLAS&H</sub>, the raw material cost, utilities cost, operating and maintenance cost, depreciation cost, plant overhead cost, and general expenses respectively account for 69%, 13%, 0.8%, 12.3%, 0.6%, and 4% of the total production cost. The price of raw coal, steam price, and total capital investment have the greatest impact on the total production cost. In this paper, we conducted sensitivity analysis on the effect of coal price, steam price, and total capital investment on the production cost.

The results are shown in Figure 19. In the case of coal prices falling and rising by 20%, the TPC of the  $CTU_{CLAS\&H}$  drops to USD 140.95/t-urea and rises to USD 183.28/t-urea, and that of the  $COG-CTU_{CLAS\&H}$  drops to USD 166.64/t-urea and rises to USD 236.03/t-urea. The steam price and total capital investment have little impact on the production cost.

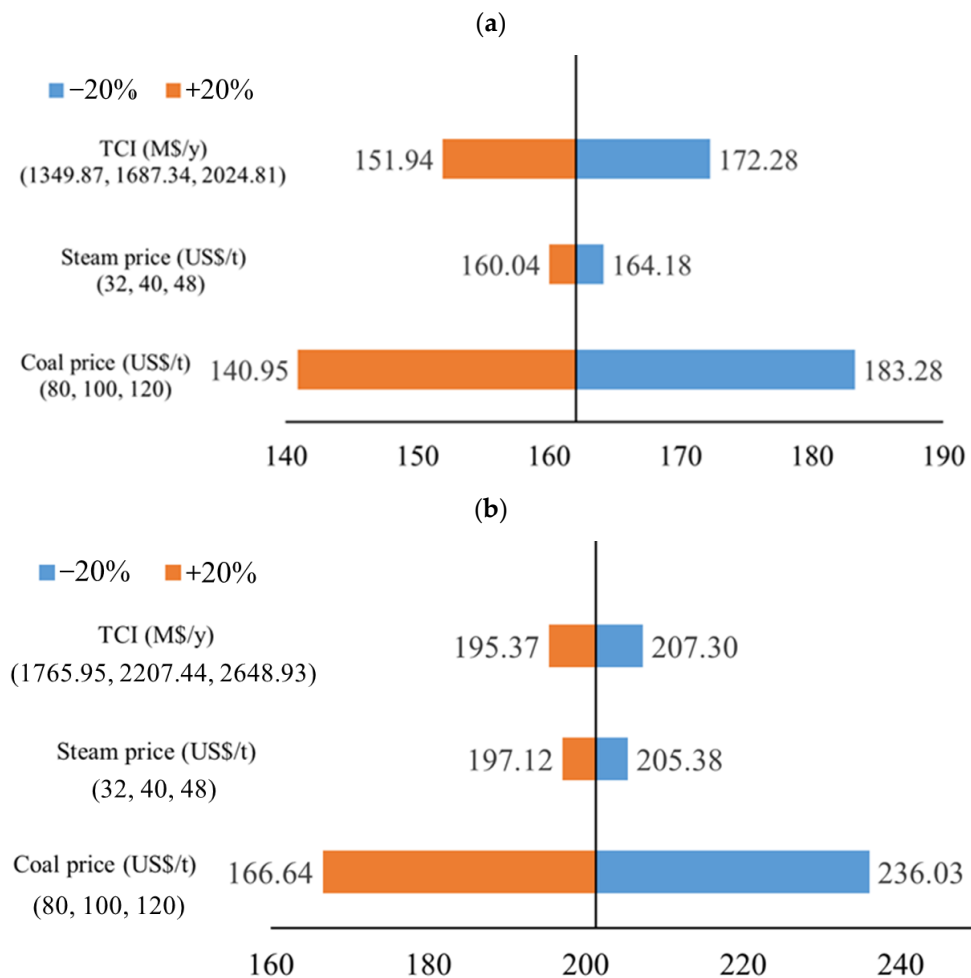


**Figure 19.** Sensitivity analysis of the effects of variables on the production cost of (a)  $CTU_{CLAS\&H}$  and (b)  $COG-CTU_{CLAS\&H}$ .

#### 4.3.4. Internal Rate of Return Analysis

The IRRs for three processes are shown in Figure 20. The IRRs of the CTU,  $CTU_{CLAS\&H}$ , and  $COG-CTU_{CLAS\&H}$  processes are 14%, 16%, and 26% with the coal and urea prices of USD 100 and USD 357/t, respectively. Obviously, the IRRs of the  $COG-CTU_{CLAS\&H}$  process are higher than those of the CTU and  $CTU_{CLAS\&H}$  processes. Moreover, the IRRs of the three processes are greater than 12%, where all three processes are economically feasible and profitable. Moreover, the IRRs for processes highly relies on the urea price. When urea price increase from USD 285 to 428/t, the IRRs of CTU,  $CTU_{CLAS\&H}$ , and  $COG-CTU_{CLAS\&H}$  processes are increased to 21%, 24%, and 39%, respectively. In addition, when coal prices increase from USD 80 to 120/t, the IRRs of different processes are decreased to 11%, 14%, and 24%, respectively.

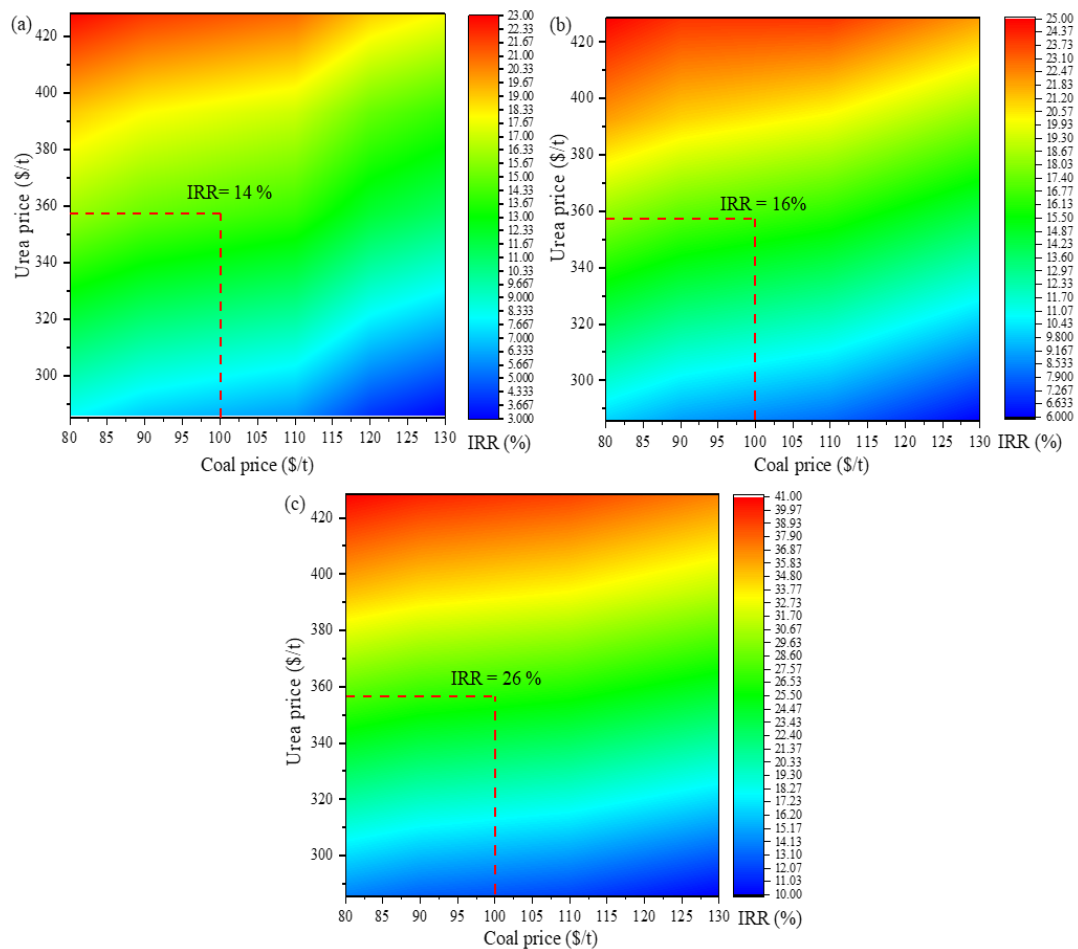


**Figure 20.** Effect of coal and urea prices on the IRRs of (a) CTU, (b)  $CTU_{CLAS\&H}$ , and (c)  $COG-CTU_{CLAS\&H}$ .

## 5. Conclusions

In this paper, two novel coal-to-urea processes ( $CTU_{CLAS\&H}$  and  $COG-CTU_{CLAS\&H}$ ) based on chemical looping air separation (CLAS) and chemical looping hydrogen production (CLH) technologies are proposed for high energy efficiency and urea yield. The high energy consumption of cryogenic air separation unit and water–gas shift unit of the traditional CTU process is replaced by CLAS and CLH in the  $CTU_{CLAS\&H}$ . Furthermore, COG feedstock is introduced into the  $CTU_{CLAS\&H}$  to improve carbon utilization efficiency and overall system energy efficiency. Technical-economic performances are assessed in this paper after process modeling, key parameter analysis, and system analysis. The main conclusions for this study are as follows:

1. The optimized oxygen/coal ratio,  $Mn_3O_4$ /air, S/ $Mn_2O_3$ ,  $Fe_2O_3$ /CG, and COG/CG are 0.7, 0.8, 0.3, 0.3, and 1.2, respectively, and 830 °C is chosen for the reaction temperature of the CLAS.
2. The carbon utilization ratio of  $COG-CTU_{CLAS\&H}$  is 78.94% higher than that of traditional CTU (35.67%) when the optimized value COG/CG is 1.2. Compared with the CTU and  $CTU_{CLAS\&H}$ , the  $COG-CTU_{CLAS\&H}$  process can generally achieve the highest overall system efficiency (77.10%), indicating a promising technical method for  $CTU_{CLAS\&H}$  assisted with COG feedstock.
3. The product costs of CTU,  $CTU_{CLAS\&H}$  and  $COG-CTU_{CLAS\&H}$  processes are USD 174.65, USD 162.11, and USD 201.34/t-urea, respectively. The introduction of coke-oven gas results in increased production cost of the  $COG-CTU_{CLAS\&H}$  process. Sensitivity analysis of the coal price and urea price changes on internal return of rate

indicates that the COG-CTU<sub>CLAS&H</sub> has higher economic benefit and stronger ability to resist market risk. The urea yield is enhanced largely improving the economic performance and market competitiveness of COG-CTU<sub>CLAS&H</sub>.

It is concluded that the COG-CTU<sub>CLAS&H</sub> process has more considerable technical and economic advantages than those of the CTU and CTU<sub>CLAS&H</sub> processes. The CLAS and CLH are the state-of-the-art technologies for lower energy consumption and lower capital investment used in the CTU process. In addition, the introduction of COG brings about a higher carbon utilization rate and larger economic benefits. However, the integration of COG pretreatment and pressure swing adsorption makes the urea production process longer and more complex, which affects the process's operability and security. This paper is focused on conceptual design and modeling of the COG-CTU<sub>CLAS&H</sub> as well as exploring its techno-economic feasibility. The next work should be conducted for optimizing material, energy, and water networks and the safety control of the whole system. Therefore, we hope this work can provide a promising route for urea production characterized by economic and environmental benefits.

**Supplementary Materials:** The following supporting information can be downloaded at: <https://www.mdpi.com/article/10.3390/pr11030960/s1>, Table S1: Ratio factors for capital investment; Table S2: Assumptions for the estimation of the total product cost; Table S3: Simulation results of the CTU process; Table S4: Simulation results of the CTU<sub>CLAS&H</sub> process; Table S5: Simulation results of the COG-CTU<sub>CLAS&H</sub> process.

**Author Contributions:** Conceptualization, Q.W. and H.Z.; methodology, Q.W.; software, Q.W.; validation, Q.W., H.Z. and Y.Y.; formal analysis, Q.W.; investigation, Q.W.; resources, H.Z.; data curation, H.Z.; writing—original draft preparation, Q.W.; writing—review and editing, Y.Y.; visualization, H.Z.; supervision, H.Z.; project administration, H.Z. All authors have read and agreed to the published version of the manuscript.

**Funding:** This research received no external funding.

**Data Availability Statement:** The data presented in this study are available on request from the first author.

**Conflicts of Interest:** The authors declare no conflict of interest.

## References

1. Sergeev, Y.A.; Anderzhanov, R.V.; Vorob'Ev, A.A. Energy- and Resource-Saving Technologies and Equipment in Urea Production. *Russ. J. Gen. Chem.* **2020**, *90*, 1168–1172. [CrossRef]
2. Rollinson, A.N.; Rickett, G.L.; Lea-Langt, A.; Dupont, V.; Twigg, M.V. Hydrogen from urea-water and ammonia-water solutions. *Appl. Catal. B Environ.* **2011**, *106*, 304–315. [CrossRef]
3. Elishav, O.; Lewin, D.R.; Shter, G.E.; Grader, G.S. The nitrogen economy: Economic feasibility analysis of nitrogen-based fuels as energy carriers. *Appl. Energy* **2017**, *185*, 183–188. [CrossRef]
4. Bicer, Y.; Dincer, I.; Vezina, G.; Raso, F. Impact Assessment and Environmental Evaluation of Various Ammonia Production Processes. *Environ. Manag.* **2017**, *59*, 842–855. [CrossRef]
5. Habgood, D.C.; Hoadley, A.F.; Zhang, L. Techno-economic analysis of gasification routes for ammonia production from Victorian brown coal. *Chem. Eng. Res. Des.* **2015**, *102*, 57–68. [CrossRef]
6. Yang, C.-J.; Jackson, R.B. China's growing methanol economy and its implications for energy and the environment. *Energy Policy* **2012**, *41*, 878–884. [CrossRef]
7. Huang, H.; Yang, S.; Cui, P. Design concept for coal-based polygeneration processes of chemicals and power with the lowest energy consumption for CO<sub>2</sub> capture. *Energy Convers. Manag.* **2018**, *157*, 186–194. [CrossRef]
8. Khan, M.N.; Shamim, T. Investigation of hydrogen generation in a three reactor chemical looping reforming process. *Appl. Energy* **2016**, *162*, 1186–1194. [CrossRef]
9. Adanez, J.; Abad, A.; Garcia-Labiano, F.; Gayan, P.; de Diego, L.F. Progress in Chemical-Looping Combustion and Reforming technologies. *Prog. Energy Combust. Sci.* **2012**, *38*, 215–282. [CrossRef]
10. Nandy, A.; Loha, C.; Gu, S.; Sarkar, P.; Karmakar, M.K.; Chatterjee, P.K. Present status and overview of Chemical Looping Combustion technology. *Renew. Sustain. Energy Rev.* **2016**, *59*, 597–619. [CrossRef]
11. Moghtaderi, B. Review of the Recent Chemical Looping Process Developments for Novel Energy and Fuel Applications. *Energy Fuels* **2011**, *26*, 15–40. [CrossRef]

12. Tong, A.; Bayham, S.; Kathe, M.V.; Zeng, L.; Luo, S.; Fan, L.-S. Iron-based syngas chemical looping process and coal-direct chemical looping process development at Ohio State University. *Appl. Energy* **2014**, *113*, 1836–1845. [[CrossRef](#)]
13. Edrisi, A.; Mansoori, Z.; Dabir, B.; Shahnazari, A. Hydrogen, nitrogen and carbon dioxide production through chemical looping using iron-based oxygen carrier—A Green plant for H<sub>2</sub> and N<sub>2</sub> production. *Int. J. Hydrog. Energy* **2014**, *39*, 10380–10391. [[CrossRef](#)]
14. Edrisi, A.; Mansoori, Z.; Dabir, B. Using three chemical looping reactors in ammonia production process—A novel plant configuration for a green production. *Int. J. Hydrog. Energy* **2014**, *39*, 8271–8282. [[CrossRef](#)]
15. Mehrpooya, M.; Sharifzadeh, M.M.M.; Rajabi, M.; Aghbashlo, M.; Tabatabai, M.; Hosseinpour, S.; Ramakrishna, S. Design of an integrated process for simultaneous chemical looping hydrogen production and electricity generation with CO<sub>2</sub> capture. *Int. J. Hydrog. Energy* **2017**, *42*, 8486–8496. [[CrossRef](#)]
16. Kim, A.R.; Lee, H.Y.; Cho, J.M.; Choi, J.-H.; Bae, J.W. Ni/M-Al<sub>2</sub>O<sub>3</sub> (M=Sm, Ce or Mg) for combined steam and CO<sub>2</sub> reforming of CH<sub>4</sub> from coke oven gas. *J. CO<sub>2</sub> Util.* **2017**, *21*, 211–218. [[CrossRef](#)]
17. Yi, Q.; Wu, G.-S.; Gong, M.-H.; Huang, Y.; Feng, J.; Hao, Y.-H.; Li, W.-Y. A feasibility study for CO<sub>2</sub> recycle assistance with coke oven gas to synthetic natural gas. *Appl. Energy* **2017**, *193*, 149–161. [[CrossRef](#)]
18. Bhui, B.; Vairakannu, P. Experimental and kinetic studies on in-situ CO<sub>2</sub> gasification based chemical looping combustion of low ash coal using Fe<sub>2</sub>O<sub>3</sub> as the oxygen carrier. *J. CO<sub>2</sub> Util.* **2019**, *29*, 103–116. [[CrossRef](#)]
19. Hao, Y.; Huang, Y.; Gong, M.; Li, W.; Feng, J.; Yi, Q. A polygeneration from a dual-gas partial catalytic oxidation coupling with an oxygen-permeable membrane reactor. *Energy Convers. Manag.* **2015**, *106*, 466–478. [[CrossRef](#)]
20. Li, S. *The Mechanism of Minimal Energy Penalty for CO<sub>2</sub> Capture and the Study on Coal-Based Polygeneration System for Cogenerating Substitute Natural Gas and Power*; Graduate University of Chinese Academy of Sciences: Beijing, China, 2012.
21. Ge, H.; Guo, W.; Shen, L.; Song, T.; Xiao, J. Biomass gasification using chemical looping in a 25 kWth reactor with natural hematite as oxygen carrier. *Chem. Eng. J.* **2016**, *286*, 174–183. [[CrossRef](#)]
22. Tagliaferri, C.; Görke, R.; Scott, S.; Dennis, J.; Lettieri, P. Life cycle assessment of optimised chemical looping air separation systems for electricity production. *Chem. Eng. Res. Des.* **2018**, *131*, 686–698. [[CrossRef](#)]
23. Shah, K.; Moghtaderi, B.; Wall, T. Effect of flue gas impurities on the performance of a chemical looping based air separation process for oxy-fuel combustion. *Fuel* **2013**, *103*, 932–942. [[CrossRef](#)]
24. Zhou, C.; Shah, K.; Song, H.; Zanganeh, J.; Doroodchi, E.; Moghtaderi, B. Integration Options and Economic Analysis of an Integrated Chemical Looping Air Separation Process for Oxy-fuel Combustion. *Energy Fuels* **2015**, *30*, 1741–1755. [[CrossRef](#)]
25. Shi, B.; Wu, E.; Wu, W.; Kuo, P.-C. Multi-objective optimization and exergoeconomic assessment of a new chemical-looping air separation system. *Energy Convers. Manag.* **2018**, *157*, 575–586. [[CrossRef](#)]
26. Zhu, L.; Wang, F.; Zhang, Z. Thermodynamic evaluation of a conceptual process for coal gasification coupled with chemical looping air separation. *Chem. Eng. Process.-Process Intensif.* **2016**, *106*, 33–41. [[CrossRef](#)]
27. Zhang, D.; Duan, R.; Li, H.; Yang, Q.; Zhou, H. Optimal design, thermodynamic, cost and CO<sub>2</sub> emission analyses of coal-to-methanol process integrated with chemical looping air separation and hydrogen technology. *Energy* **2020**, *203*, 117876. [[CrossRef](#)]
28. Xiang, D.; Zhao, S. Parameter optimization and thermodynamic analysis of COG direct chemical looping hydrogen processes. *Energy Convers. Manag.* **2018**, *172*, 1–8. [[CrossRef](#)]
29. Qin, S.; Chang, S.; Yao, Q. Modeling, thermodynamic and techno-economic analysis of coal-to-liquids process with different entrained flow coal gasifiers. *Appl. Energy* **2018**, *229*, 413–432. [[CrossRef](#)]
30. Zhou, H.; Yang, S.; Xiao, H.; Yang, Q.; Qian, Y.; Gao, L. Modeling and techno-economic analysis of shale-to-liquid and coal-to-liquid fuels processes. *Energy* **2016**, *109*, 201–210. [[CrossRef](#)]
31. Wang, D.; Meng, W.; Zhou, H.; Yang, Y.; Xie, J.; Yang, S.; Li, G. Novel coal-to-methanol process with near-zero carbon emission: Pulverized coal gasification-integrated green hydrogen process. *J. Clean. Prod.* **2022**, *339*, 130500. [[CrossRef](#)]
32. Kuo, P.-C.; Wu, W. Thermodynamic analysis of a combined heat and power system with CO<sub>2</sub> utilization based on co-gasification of biomass and coal. *Chem. Eng. Sci.* **2016**, *142*, 201–214. [[CrossRef](#)]
33. Hacker, V.; Fankhauser, R.; Faleschini, G.; Fuchs, H.; Friedrich, K.; Muhr, M.; Kordesch, K. Hydrogen production by steam-iron process. *J. Power Sources* **2000**, *86*, 531–535. [[CrossRef](#)]
34. Zheng, T.; Li, M.; Mei, D.; Ma, J.; Wang, B.; Xu, Z. Effect of H<sub>2</sub>S presence on chemical looping reforming (CLR) of biogas with a firebrick supported NiO oxygen carrier. *Fuel Process. Technol.* **2022**, *226*, 107088. [[CrossRef](#)]
35. de Diego, L.F.; Ortiz, M.; García-Labiano, F.; Adánez, J.; Abad, A.; Gayán, P. Hydrogen production by chemical-looping reforming in a circulating fluidized bed reactor using Ni-based oxygen carriers. *J. Power Sources* **2009**, *192*, 27–34. [[CrossRef](#)]
36. Morud, J.C.; Skogestad, S. Analysis of instability in an industrial ammonia reactor. *AIChE J.* **1998**, *44*, 888–895. [[CrossRef](#)]
37. Flórez-Orrego, D.; de Oliveira Junior, S. Modeling and optimization of an industrial ammonia synthesis unit: An exergy approach. *Energy* **2017**, *137*, 234–250. [[CrossRef](#)]
38. Xiang, D.; Zhou, Y. Concept design and techno-economic performance of hydrogen and ammonia co-generation by coke-oven gas-pressure swing adsorption integrated with chemical looping hydrogen process. *Appl. Energy* **2018**, *229*, 1024–1034. [[CrossRef](#)]
39. Araújo, A.; Skogestad, S. Control structure design for the ammonia synthesis process. *Comput. Chem. Eng.* **2008**, *32*, 2920–2932. [[CrossRef](#)]
40. Meessen, J. Urea synthesis. *Chem. Ing. Tech.* **2014**, *86*, 2180–2189. [[CrossRef](#)]

41. Yang, Q.; Zhang, Z.; Fan, Y.; Chu, G.; Zhang, D.; Yu, J. Advanced exergy analysis and optimization of a CO<sub>2</sub> to methanol process based on rigorous modeling and simulation. *Fuel* **2022**, *325*, 124944. [[CrossRef](#)]
42. Zhang, J.; Yang, Q.; Fan, Y.; Zhang, D.; Yu, J. Conceptual design and techno-economic analysis of a coproduction system for ethylene glycol and LNG from steel mill off-gases. *Fuel* **2022**, *318*, 123693. [[CrossRef](#)]
43. Xiang, D.; Xiang, J.; Sun, Z.; Cao, Y. The integrated coke-oven gas and pulverized coke gasification for methanol production with highly efficient hydrogen utilization. *Energy* **2017**, *140*, 78–91. [[CrossRef](#)]
44. Wang, D.; Meng, W.; Zhou, H.; Li, G.; Yang, Y.; Li, H. Green hydrogen coupling with CO<sub>2</sub> utilization of coal-to-methanol for high methanol productivity and low CO<sub>2</sub> emission. *Energy* **2021**, *231*, 120970.
45. Kathe, M.V.; Empfield, A.; Na, J.; Blair, E.; Fan, L.-S. Hydrogen production from natural gas using an iron-based chemical looping technology: Thermodynamic simulations and process system analysis. *Appl. Energy* **2016**, *165*, 183–201. [[CrossRef](#)]

**Disclaimer/Publisher's Note:** The statements, opinions and data contained in all publications are solely those of the individual author(s) and contributor(s) and not of MDPI and/or the editor(s). MDPI and/or the editor(s) disclaim responsibility for any injury to people or property resulting from any ideas, methods, instructions or products referred to in the content.